
CMS Physics Analysis Summary

Contact: cms-pag-conveners-higgs@cern.ch

2019/03/17

Search for neutral MSSM Higgs bosons decaying to $\mu^+\mu^-$ in pp collisions at $\sqrt{s} = 13$ TeV

The CMS Collaboration

Abstract

A search for neutral non-standard-model Higgs bosons decaying to two muons is presented. The search is performed in the context of the minimal supersymmetric standard model, using proton-proton collisions data recorded by CMS at the CERN Large Hadron Collider at a center-of-mass energy of 13 TeV. The integrated luminosity is 35.9 fb^{-1} . The search is sensitive to neutral Higgs bosons produced via gluon fusion process or in association with a $b\bar{b}$ quark pair. No significant deviation from the standard model expectation is observed. A 95% confidence level upper limit is set in the context of the $m_h^{\text{mod+}}$ and hMSSM scenarios on the parameter $\tan\beta$ as a function of the pseudoscalar A boson mass, in the range from 130 to 600 GeV. The larger collected luminosity and the higher center-of-mass energy exclude a larger $m_A\text{-}\tan\beta$ region, compared to what was obtained at 7 and 8 TeV by a similar analysis. The results are also used to set a model-independent limit on the product of the branching fraction for the decay into a muon pair and the cross section for the production of a scalar neutral boson, either via gluon fusion, or in association with b quarks, in the mass range from 130 to 1000 GeV.

1 Introduction

The scalar boson with a mass of 125.09 ± 0.21 (stat) ± 0.11 (syst) GeV, discovered at the CERN Large Hadron Collider (LHC) in 2012 [1–3], has properties that are well-consistent with those predicted for the standard model (SM) Higgs boson [4, 5]. However, the SM is known to be incomplete, and several well-motivated theoretical models beyond the SM predict an extended Higgs sector. One example is supersymmetry [6, 7] that protects the mass of the Higgs boson against quadratically divergent quantum corrections. In the minimal supersymmetric standard model (MSSM) [8–10], the Higgs sector consists of two Higgs doublets, one of which couples to up-type fermions and the other to down-type fermions. Assuming that CP symmetry is conserved, this results in two charged bosons H^\pm , two neutral scalar bosons, h and H , and one pseudoscalar boson, A . In this note, the term Higgs boson will be used to refer to neutral Higgs bosons beyond the SM, unless explicitly specified.

At the tree level, the Higgs sector in the MSSM can be described by only two parameters, which are commonly chosen as m_A , the mass of the neutral A , and $\tan\beta$, the ratio of the vacuum expectation values of the neutral components of the two Higgs doublets. The masses of the other four Higgs bosons can be expressed as a function of these two parameters. Beyond the tree level, the MSSM Higgs sector depends on additional parameters, which enter via higher-order corrections in perturbation theory, and which are usually fixed to values motivated by experimental constraints and theoretical assumptions. Setting these parameters defines a benchmark scenario [11], which is then described by m_A and $\tan\beta$. The relevant scenarios are those consistent with a mass of one neutral boson of 125 GeV for the majority of the probed m_A - $\tan\beta$ parameter space [12], and not ruled out by other existing measurements. In particular, the $m_h^{\text{mod}+}$ scenario [13] constrains the mass of the h boson near 125 GeV for a wide range of $\tan\beta$ and m_A values. The phenomenological hMSSM model [14–16] also incorporates the observed neutral boson at 125 GeV, interpreting it as the h boson.

This note reports on a search for beyond-the-SM neutral Higgs bosons in the dimuon final state in proton proton (pp) collisions at a center-of-mass energy ($\sqrt{s} =$) of 13 TeV. The search is performed in the context of the MSSM, assuming either the $m_h^{\text{mod}+}$ or the hMSSM scenario. The search for the two neutral Higgs bosons H and A is performed by hunting for dimuon resonances with invariant mass values larger than 130 GeV. The light h boson is expected to have a mass consistent with that of the already observed Higgs boson within a few GeV. Alternatively, the search is also performed in a model-independent way, where the neutral boson is assumed to be produced either via the gluon fusion or the b associated production mechanisms.

At LHC, dominant production mechanisms for neutral MSSM Higgs bosons are gluon fusion, where the Higgs boson can be produced via a virtual loop of bottom or top quarks, and b associated production, where the Higgs bosons is produced in association with a b quark pair. Figure 1 shows the Feynman diagrams of the two production processes given at leading order (LO). The gluon fusion mechanism is more relevant for $\tan\beta \lesssim 30$, whereas at LO, the coupling of the Higgs boson to down-type fermions is enhanced by $\tan\beta$, resulting in b associated production becoming more important at large $\tan\beta$. The coupling of the neutral Higgs boson to charged leptons is enhanced for the same reason. Although the branching fraction to muons is predicted to be about 300 times smaller than that for the $\tau^+\tau^-$ final state, the $\mu^+\mu^-$ channel can be fully reconstructed, and the dimuon invariant mass can be measured with a precision of a few percent by exploiting the excellent muon momentum resolution of the CMS detector, making the dimuon final state an additional probe of the MSSM.

The common experimental signature of the two production mechanisms is a pair of opposite-charge muons with high transverse momentum (p_T). The b associated production process

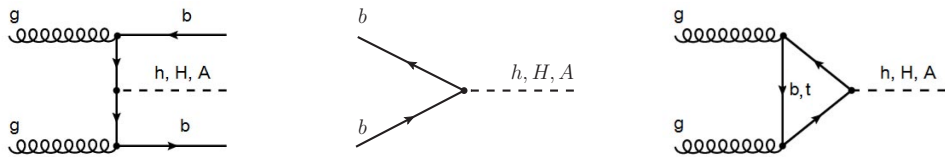


Figure 1: Leading order diagrams of the MSSM Higgs bosons production at the LHC: the b associated production (left and middle), and the gluon fusion production (right).

is characterized by the presence of additional jets originating from b quark fragmentation, whereas the events containing jets from light quarks or gluons are linked to the gluon fusion production mechanism. The presence of a signal would be characterized by an excess of events over the SM background in the dimuon invariant mass corresponding to the value of the Higgs boson masses.

The analysis is performed using the data at $\sqrt{s} = 13$ TeV collected during 2016 by the CMS experiment at the LHC corresponding to an integrated luminosity of 35.9 fb^{-1} . Similar searches in the dimuon final state were performed by the ATLAS and CMS Collaborations using data collected in pp collisions at $\sqrt{s} = 7$ and 8 TeV [17, 18], and by ATLAS at $\sqrt{s} = 13$ TeV [19]. Searches for neutral Higgs bosons in the framework of the MSSM were performed by the ATLAS and CMS experiments also in the $\tau^+\tau^-$ [17, 20–25] and $b\bar{b}$ [26–28] final states. Limits on the existence of the MSSM Higgs bosons were determined also in e^+e^- collisions at $\sqrt{s} = 91$ – 209 GeV at the CERN LEP [29] and in proton-antiproton collisions at $\sqrt{s} = 1.96$ TeV at the Fermilab Tevatron [30–33].

2 The CMS detector

The central feature of the CMS apparatus is a superconducting solenoid of 6 m internal diameter, providing a field of 3.8 T. Within the field volume are a silicon pixel and strip tracker, a crystal electromagnetic calorimeter, and a brass and scintillator hadron calorimeter, each composed of a barrel and two endcap sections. Muons are measured in gas-ionization detectors embedded in the steel return yoke of the magnet. The first level (L1) of the CMS trigger system uses information from the calorimeters and muon detectors to select events of interest. The high-level trigger processor farm decreases the L1 accept rate from around 100 kHz to about 1 kHz before data storage. A more detailed description of the CMS detector, together with a description of the coordinate system and main kinematic variables used in the analysis, can be found in Ref. [34].

3 Signal and background simulation

Samples of Monte Carlo (MC) simulated events are generated to model the Higgs bosons signal for the two leading production processes. This is done for a large number of m_A and $\tan\beta$ combinations, where m_A spans the range from 130 to 1000 GeV and $\tan\beta$ is varied from 5 to 60. The signal samples are generated with PYTHIA 8.212 [35] at LO. Simulated background processes are used to optimize the event selection, but not to model the background shape and normalization, which is determined directly from data. The most relevant SM background processes considered are Drell–Yan (DY) production, and single and pair production of top quarks, which can produce $\mu^+\mu^-$ pairs with large invariant mass. Other background sources are the diboson production processes, $W^\pm W^\mp$, $W^\pm Z$, and ZZ , whose contributions

are each smaller than 1% for dimuon invariant masses larger than 130 GeV, where the Higgs boson signal is searched for. The background samples are generated at next-to-LO (NLO) using `MADGRAPH5_aMC@NLO` [36] and `POWHEG 2.0` [37]. Spin correlations in multiboson processes generated using `MADGRAPH5_aMC@NLO` are simulated using `MADSPIN` [38]. The `NNPDF 3.0` [39] parton distribution functions (PDFs) are used for all samples. The parton shower and hadronization processes are modeled by `PYTHIA` with the `CUETP8M1` [40] underlying event tune.

Detector response is based on a detailed description of the CMS detector and is simulated with the `GEANT4` package [41]. Additional pp interactions within the same or nearby bunch crossing of the event of interest (pileup) are simulated by `PYTHIA`. During the data taking period, the CMS experiment was operating with, on average, 23 inelastic pp collisions per bunch crossing. The distribution of the number of additional interactions per bunch crossing in the simulation is weighted to match that observed in the data.

The values of the Higgs boson masses, widths, and the Yukawa couplings for the $m_h^{\text{mod+}}$ scenario, are calculated as a function of m_A and $\tan\beta$ using the `FEYNHIGGS 2.12.0` [42–46] program, following the LHC Cross Section Working Group prescriptions [47, 48]. Cross section and branching fractions of the Higgs bosons are taken from Ref. [47]. Cross sections for the $t\bar{t}$ and DY background processes are computed at the next-to-NLO with `TOP++2.0` [49] and `FEWZ3.1` [50], respectively, while for the single top and the diboson production processes they are computed and at NLO with `HATHOR` [51, 52] and `MCFM` [53], respectively.

4 Object reconstruction and event selection

The particle-flow (PF) algorithm [54] aims to reconstruct and identify each individual particle in an event, with an optimized combination of information from the various elements of the CMS detector. The energy of photons is obtained from the ECAL measurement. The energy of electrons is determined from a combination of the electron momentum at the primary interaction vertex as determined by the tracker, the energy of the corresponding ECAL cluster, and the energy sum of all bremsstrahlung photons spatially compatible with originating from the electron track. The energy of muons is obtained from the curvature of the corresponding track. The energy of charged hadrons is determined from a combination of their momentum measured in the tracker and the matching ECAL and HCAL energy deposits, corrected for zero-suppression effects and for the response function of the calorimeters to hadronic showers. Finally, the energy of neutral hadrons is obtained from the corresponding corrected ECAL and HCAL energies.

Muons with $20 < p_T < 100$ GeV are measured with a relative p_T resolution of 1.3 to 2% in the barrel and better than 6% in the endcaps. The p_T resolution in the barrel is better than 10% for muons with p_T up to 1 TeV [55, 56].

Jets are reconstructed using the anti- k_T clustering algorithm [57] with a distance parameter of 0.4, as implemented in the `FASTJET` package [58]. The quantity p_T^{miss} is defined as the magnitude of the negative vector p_T sum of all the PF objects (charged and neutral) in the event, and is modified by corrections to the energy scale of reconstructed jets. Collision vertices are obtained from reconstructed tracks using a deterministic annealing algorithm [59]. The reconstructed vertex with the largest value of summed physics-object p_T^2 is taken to be the primary pp interaction vertex (PV). The physics objects are the jets, clustered using the jet finding algorithm [58, 60] with the tracks assigned to the vertex as inputs, and the associated missing transverse momentum taken as the negative vector sum of the p_T of those jets.

The CSVv2 algorithm of Ref. [61] that reconstructs secondary vertices is used to identify jets resulting from the hadronization of b quarks. The algorithm is applied to jets with $p_T > 20$ GeV in the pseudorapidity range $|\eta| < 2.4$. For jets within this kinematic range, the efficiency of the algorithm is 66% with a misidentification probability of 1% for the medium working point.

The events are preselected by the trigger system [62] requiring a muon candidate with $|\eta| < 2.4$, satisfying at least one of the following criteria: $p_T > 24$ GeV with online isolation (on_iso) requirements, or $p_T > 50$ GeV without on_iso requirements. These are the trigger algorithms with the lowest p_T threshold whose output is not artificially reduced to limit the event rate, and that cover the entire η acceptance of the muon detector. Since the Higgs boson signal is searched for over a large mass range, the p_T of the muons from its decay can vary from tens to hundreds of GeV. Therefore, two sets of muon identification (ID) criteria are employed in the analysis: one is optimized for muons with lower p_T ($p_T \lesssim 200$ GeV) (ID1) and the other for muons with larger p_T (ID2).

Events with a pair of opposite-charge muons, coming from the PV, are selected requiring both muons to satisfy the same ID criterion. Accepting, more generally, pairs of muons that pass any of the two ID criteria would lead to a negligible increase in signal efficiency. At least one of the two muon candidates has to match in azimuthal angle and η the muon that triggered the event. The offline reconstructed muons with $|\eta| < 2.4$ are considered. Their offline transverse momentum is required to be $p_T > 26$ GeV or $p_T > 53$ GeV, to be compatible with muon that triggered the event. To reject muons from nonprompt decays, muon candidates must be isolated. The offline isolation variable (off_iso) is calculated depending on the ID algorithm. For ID1 it is the scalar p_T sum of the PF charged and neutral hadrons in a cone of radius $\Delta R = \sqrt{(\Delta\eta)^2 + (\Delta\phi)^2} = 0.4$ around the muon direction, and divided by the muon p_T . The charged PF particles not associated with the PV are not considered in this sum, and a correction is applied in order to account for the neutral particle contamination arising from pileup [63]. For ID2 the offline isolation variable is computed as the scalar p_T sum of tracks in the silicon tracker, excluding the muon, in a cone of radius $\Delta R = 0.3$ around the muon direction, and divided by the muon p_T . Tracks not associated with the PV are not considered. The energy deposits in the calorimeters are not included, since electromagnetic showers can develop from photons radiated by a high- p_T muon. The invariant mass of the Higgs boson candidate is reconstructed from the two highest- p_T opposite-charge muon candidates in the event.

The muon momentum measurement is crucial for the reconstruction of the Higgs boson mass peaks since improving the dimuon mass resolution in the data increases the sensitivity of the analysis. To set limits accurately, the mean and the resolution of the dimuon mass peaks in simulation must match those of the data. Therefore a correction of the muon momentum has been applied in order to provide consistent measurements in the different ϕ and η regions of the detector, improving the net resolution in data. The correction [64] is also applied to the simulated muons to align the scale and resolution to those measured in the data. The magnitudes of the momentum scale corrections are about 0.2% and 0.3% in the barrel and endcaps, respectively, for muons with p_T up to 200 GeV. For muons with larger p_T , since the statistic in data is too poor to derive a correction, only a systematic uncertainty is considered (see Sec.5).

When the Higgs boson is produced in association with a $b\bar{b}$ pair, additional jets from b quark fragmentation are expected. Jets with $p_T > 20$ GeV and $|\eta| < 2.4$ are considered in this analysis: those which satisfy the requirements for the medium b tagging working point are taken as b jet candidates, otherwise they are taken as untagged jets. Events containing b jet candidates provide the highest sensitivity for the b associated production channel, events that do not con-

tain b-tagged jets provide the best sensitivity for the gluon fusion production channel. The events are therefore split into two exclusive categories: the b tag category, containing events with strictly one b jet and at most one additional untagged jet, and the no b tag category, containing events without b-tagged jets. In the first category, the requirement of strictly one b jet is aimed at suppressing the dominant background from top quark pairs, since the observed b-tagged jet multiplicity in $t\bar{t}$ events is on average higher than for the Higgs boson signal. This is because more than half of the signal events from b associated production are characterized by b jets emitted at large η , out of the acceptance of the tracking detector, and failing the b tag requirements, whereas b jets in $t\bar{t}$ events are preferentially emitted in the central η region. Therefore, discarding events with two or more b-tagged jets allows to reject $t\bar{t}$ background with no major impact on the signal efficiency. Furthermore, $t\bar{t}$ events are characterized by a higher multiplicity of additional untagged jets than the signal events.

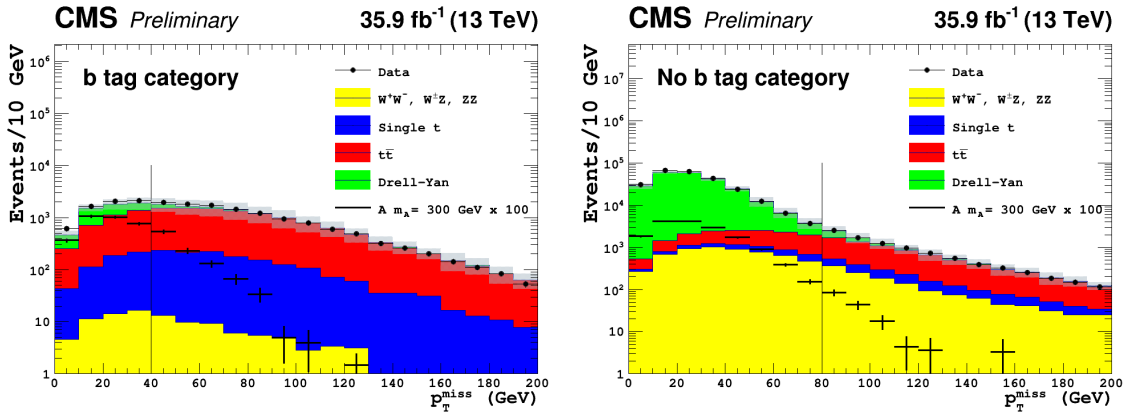


Figure 2: Distribution of the missing transverse momentum in (left) b tag and (right) no b tag categories, for events with dimuon invariant mass larger than 130 GeV, as observed in data (dots) and predicted by simulation (colored histograms). The shaded gray band around the total background histogram represents the total uncertainty in the simulated prediction. The contribution of the expected signal for $m_A = 300$ GeV and $\tan\beta = 20$, scaled by a factor of 100, is superimposed for illustration. The vertical line represents the upper threshold used to select the events in the two categories.

Signal events are characterized by a rather small p_T^{miss} . However, the background content is quite different for the two categories, as shown in Fig. 2. The background from $t\bar{t}$ events, characterized by a relatively large p_T^{miss} from W boson decays, is much more relevant for the b tag category. For the no b tag category, the dominant background is DY production, whose events are characterized by a p_T^{miss} distribution that is similar to that of the signal. For this reason, an upper requirement on p_T^{miss} , separately tuned for the b tag and the no b tag events, improves the background rejection and increases the signal sensitivity. Events belonging to the b tag (no b tag) category are required to have $p_T^{\text{miss}} < 40$ (80) GeV. The selection criteria that define the two categories are summarized in Table 1.

5 Signal efficiency and signal systematic uncertainties

Higgs boson events generated with a mass within $\pm 3\Gamma$ of the nominal Higgs boson mass, where Γ is the intrinsic width, are considered in this analysis. They are normalised to the luminosity of the data using the theoretical cross section from[46], which corresponds to the production cross-section of on-shell bosons. The values of Γ strongly depend on m_A and $\tan\beta$, being, for

Table 1: Summary of the selection criteria that define the two event categories.

| Muon selection | muon ID1 | muon ID2 |
|-----------------------|--|---|
| Online selection | $ \eta < 2.4$ | $ \eta < 2.4$ |
| Single muon | $p_T > 24 \text{ GeV, on_iso}$ | $p_T > 50 \text{ GeV}$ |
| Offline selection | $ \eta < 2.4$ | $ \eta < 2.4$ |
| Opposite-charge muons | $p_T > 26 \text{ GeV}$ $\text{off_iso} < 0.25$ | $p_T > 53 \text{ GeV}$ $\text{off_iso} < 0.1$ |
| Category selection | b tag category | No b tag category |
| b-tagged jets | 1 with $p_T > 20 \text{ GeV, } \eta < 2.4$ | veto |
| Untagged jets | 0,1 with $p_T > 20 \text{ GeV, } \eta < 2.4$ $p_T^{\text{miss}} < 40 \text{ GeV}$ | $< 80 \text{ GeV}$ |

example, $\Gamma = 0.2$ (2.7)% of the nominal Higgs boson mass at $m_A = 150$ (550) GeV and $\tan \beta = 10$ (40). For each value of m_A and $\tan \beta$, the signal efficiency of each Higgs boson sample is defined as the fraction of events in this mass interval that fulfill the selection criteria. This definition of efficiency also includes the effects of limited detector acceptance and the selections outlined in Section 4.

Figure 3 shows the selection efficiency of the A boson as a function of m_A , for the gluon fusion and the b associated production processes, and for the two event categories. For a given mass, the selection efficiency is weakly dependent on $\tan \beta$, since this parameter mostly affects the Higgs boson width, with a negligible impact on the kinematic properties of the event. Each curve corresponds to the mean of the efficiency obtained by varying $\tan \beta$ between 5 and 60, while the band of each curve corresponds to the efficiency variations combined with the statistical uncertainty of the simulated samples. The efficiency to detect events produced in association with b quarks is approximately 10% at high masses for the b tag category. This value is mostly determined by the large fraction of b jets that are emitted with a η value that is outside the coverage of the tracking detectors, and indeed about $\approx 50\%$ of events from b associated samples are reconstructed in the no b tag category. The efficiency to detect events from gluon fusion reaches a maximal value at $\approx 65\%$ for $m_A \gtrsim 400 \text{ GeV}$. The very small but nonvanishing efficiency for signal produced via gluon fusion in the b tag category is due to the b misidentification probability, which is about 1%. The corresponding efficiencies for the H boson are consistent with those shown in Fig. 3.

The systematic uncertainties on the signal description arise from a possible mismodeling of the signal efficiency, of the signal shape, and, for the model interpretation, from uncertainties on its cross-section.

The systematic uncertainties that affect the signal efficiency are given in Table 2. The size of the simulated signal samples introduces a statistical uncertainty in the signal efficiency that is between 0.2% and 6%, depending on the number of generated events.

In order to account for the differences between data and simulation in the muon trigger efficiency, identification, and isolation, scale factors calculated using the tag-and-probe technique [55, 56] have been applied to simulated events. A similar procedure is used to account for discrepancies between data and simulation in the b tagging efficiency. A global correction, calculated as the product of the various scale factors, is applied as an event-by-event weight. The

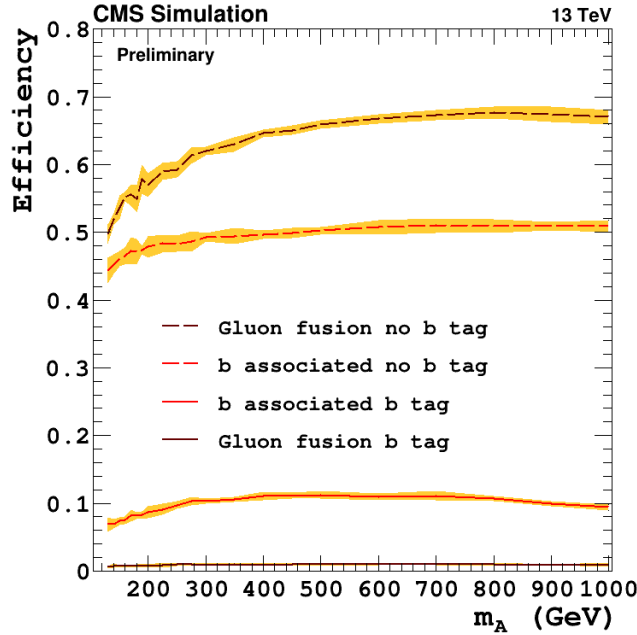


Figure 3: The selection efficiency of the A boson, as a function of its mass, for the two production mechanisms, b associated and gluon fusion, and for each of the two event categories. The band of each curve corresponds to the efficiency variations observed when varying $\tan \beta$, combined with the statistical uncertainty.

uncertainty associated with each scale factor is then propagated to the analysis and its impact on the final selection efficiency is assigned as systematic uncertainty. An event-by-event weight is also applied to account for the modeling of the pileup in the simulation. The uncertainty in the knowledge of the pileup multiplicity is evaluated by varying the total inelastic cross section [65, 66] by $\pm 5\%$, which translates into an uncertainty smaller than 1% in the signal efficiency. The uncertainty associated with the jet energy scale [67] is estimated by rescaling the jet momentum by a factor depending on the p_T and η of each jet. This variation is also propagated to the p_T^{miss} determination. Its effect on the signal selection efficiency is about 1.6% (0.4%) for the b tag (no b tag) category. Systematic uncertainties in the unclustered energy are propagated to the determination of p_T^{miss} . The effect on the signal efficiency is 4.1% for the b tag category, and 0.3% for the no b tag category. The uncertainty in the total integrated luminosity is 2.5% [68].

The uncertainties in the MSSM cross sections depend on m_A , $\tan \beta$, and the scenario. They are provided by the LHC Cross Section Working Group [47, 48]. The set of PDFs used to generate the Higgs boson signals is the NNPDF 3.0 and an uncertainty of 3% in the signal efficiency has been accounted for them.

Additional corrections are applied to take into account the fact that the signal samples are generated with PYTHIA at LO instead of using a NLO generator. Higher-order corrections affect the Higgs boson p_T modeling, with impact on the muon acceptance and the jet multiplicity. Moreover, they cause event migration between the two categories. These effects are accounted for using signal samples generated at NLO (such samples were generated for some mass points only though covering the whole mass range). The acceptance obtained from the LO samples is corrected to that predicted at NLO. The corresponding systematic uncertainty is set to the size of the correction itself. The correction on the modeling of the Higgs p_T is estimated using gluon fusion samples produced with POWHEG, and it increases the signal efficiency by 1–4%, depend-

Table 2: Systematic uncertainties in the signal selection efficiency for the two event categories. The systematic uncertainties hold for both Higgs boson production processes except for the sources listed in the last three rows, which apply to the b associated production process only. For these three sources, in the model-independent search for a neutral boson produced in association with b quarks, the uncertainties are applied as quoted in the table. In the MSSM interpretation, these numbers have to be weighted by the relative contribution of the b associated production process to each category. For those sources of systematics that depend from m_A the range of uncertainty is quoted.

| Source | Systematic uncertainty (%) | |
|--|----------------------------|----------|
| | b tag | no b tag |
| MC statistical uncertainty | 0.5–6 | 0.2–2 |
| Trigger efficiency | 0.9 | 0.9 |
| Muon reconstruction | 2 | 2 |
| Muon isolation | 1 | 2 |
| Pileup | 0.8 | 0.9 |
| Jet energy scale | 1.6 | 0.4 |
| Unclustered energy | 4.1 | 0.3 |
| Integrated luminosity | 2.5 | 2.5 |
| PDF | 3 | 3 |
| Higgs boson p_T | 1–4 | 1–4 |
| b tag (only for b associated production) | 2 | 0.6 |
| b jet multiplicity (only for b associated production) | 20–30 | 7–20 |
| Untagged jet multiplicity (only for b associated production) | 7–25 | — |

ing on the Higgs boson mass. The correction on the b jet multiplicity is estimated by comparing the b associated production samples produced with PYTHIA and MADGRAPH5_aMC@NLO. This affects only the b associated signal, resulting in a correction of 20–30% depending on m_A , which increases the signal efficiency for the b tag category, and a correction of 7–20% decreasing the signal efficiency for the no b tag category. An additional correction of 7–25%, related to the untagged jet multiplicity, is applied, and reduces the signal efficiency for the b tag category, due to the veto on the untagged jets.

The systematic uncertainties on the b tag efficiency and the jet multiplicity shown in Table 2 apply only to the b associated production process. In the model-independent analysis for the case when the neutral boson is assumed to be entirely produced in association with b quarks, these uncertainties are applied, as quoted in Table 2. The b tagging and the b jet multiplicity uncertainties are anticorrelated between the two event categories. In the MSSM interpretation, where both the gluon fusion and the b associated production processes contribute to the two event categories, these systematic uncertainties are weighted by the relative contribution of the latter process.

The shape of the reconstructed Higgs boson invariant mass is affected by the muon momentum scale and resolution. Uncertainties in the calibration of these quantities are propagated to the shape of the invariant mass distribution assuming a Gaussian distribution, yielding maximal variations up to 10% in its width. These uncertainties are taken into account as a signal shape variation in the calculation of the exclusion limit.

6 Modeling of the signal and background shapes

The invariant mass spectrum of the signal events that pass the event selection is used to determine the signal yield of each category. In the framework of the MSSM, this is done by fitting the invariant mass distribution of the h , H , and A bosons, separately for the two event categories and for various combinations of m_A – $\tan\beta$ values. The function F_{sig} used to parametrize the signal mass shape [18] is defined as:

$$F_{\text{sig}} = w_h \cdot F_h + w_H \cdot F_H + w_A \cdot F_A. \quad (1)$$

In Eq. (1), the terms F_h , F_H , and F_A describe the mass shape of the h , H , and A signals, respectively. Each term is a convolution of a Breit–Wigner (BW) function to describe the signal resonance, with a Gaussian function to account for the detector resolution. The two parameters of the BW function, as well as the variance of each Gaussian function, are free parameters of the fit, while the quantities w_h , w_H , and w_A are the numbers of expected events of each boson passing the event selection. For the m_A – $\tan\beta$ points for which the signal samples were not generated, the parameters are interpolated from the nearby generated points. In order to correct for differences of the order of a few GeV between the PYTHIA prediction of m_H with respect to the value calculated by FEYNHIGGS, especially for $m_A \lesssim 200$ GeV, the invariant mass distribution of the H boson is shifted by the corresponding amount.

The analysis does not use background estimation from simulation due to the limited size of simulated events compared to data in the region of interest, as well as due to the large theoretical uncertainties in the background description at high invariant masses. Therefore, given the smooth dependence of the background shape on the dimuon invariant mass, it is estimated from the data, by assuming a functional form to describe its dependence as a function of the reconstructed dimuon invariant mass, $m_{\mu\mu}$, and by fitting it to the observed distribution.

The functional form used to describe the background shape is defined as:

$$F_{\text{bkg}} = \exp(\lambda m_{\mu\mu}) \left[\frac{f}{N_1} \cdot \frac{1}{(m_{\mu\mu} - m_Z)^2 + \frac{\Gamma_Z^2}{4}} + \frac{(1-f)}{N_2} \cdot \frac{1}{m_{\mu\mu}^2} \right]. \quad (2)$$

The quantity $\exp(\lambda m_{\mu\mu})$ parametrizes the exponential part of the mass distribution, and f represents the weight of the BW term with respect to photon exchange, while N_1 and N_2 correspond to the integral of each term in F_{bkg} . The quantities λ and f are free parameters of the fit. The parameters Γ_Z and m_Z are separately determined for the two event categories by fitting the dimuon mass distribution close to the Z boson mass. The fit provides the effective values of such quantities, which include detector and resolution effects. Their values are then kept constant when using F_{bkg} in the final fit. The systematic uncertainty that stems from the choice of the functional form in Eq. (2), which was used in earlier searches [18], is assessed as described below.

A linear combination of the functions describing the expected signal and the background is then used to perform a binned maximum likelihood fit to the data, where the uncertainties are treated as nuisance parameters:

$$F_{\text{fit}} = (1 - f_{\text{bkg}}) \cdot F_{\text{sig}} + f_{\text{bkg}} \cdot F_{\text{bkg}}. \quad (3)$$

The maximization of the likelihood is performed for each m_A and $\tan\beta$ hypothesis, as the yield of the signal events and the shape of F_{sig} depends on these quantities. The parameters that describe the signal are determined by fitting the simulated samples that pass the event selection

with Eq. (1), for each m_A and $\tan \beta$ pair, as explained above. Subsequently they are assigned as constant terms in F_{fit} . The quantity f_{bkg} is a free parameter in the fit, and the fraction of signal events is defined as $f_{\text{sig}} = (1 - f_{\text{bkg}})$. The overall normalization is also a free parameter and it is profiled in the fit.

For each m_A assumption, the function F_{fit} is used to fit the data over a $m_{\mu\mu}$ range centered on m_A . The range has to be large enough to account for the signal width, including the experimental resolution, and it is $\pm 50 \text{ GeV}$, if $m_A < 290 \text{ GeV}$, $\pm 75 \text{ GeV}$, for $290 < m_A < 390 \text{ GeV}$, and $\pm 100 \text{ GeV}$, for $390 < m_A < 500 \text{ GeV}$. For $m_A > 500 \text{ GeV}$, the entire range from 400 to 1200 GeV is used.

The uncertainty introduced by the choice of the analytical function that is used to parametrize the background is estimated by using a method similar to that used in Refs.[3, 18, 69]. The method is based on the determination of the number of spurious signal events that are introduced by the choice of the background function F_{bkg} , when the background is fit by the function F_{fit} . The invariant mass spectrum is fitted by the function F_{bkg}^a , chosen among various functional forms: Eq. (2) or other similar expressions that include a BW plus exponentials, and sum of exponentials. All those functional forms adequately describe the background distribution observed in data. The fit is performed in the proper mass range centered around the assumed value of m_A , and the parameters of F_{bkg}^a are determined. Then, thousands MC pseudo-experiments are generated, each one containing the same number of events as observed in the data, distributed according to the functional form F_{bkg}^a . For each pseudo-experiment, the invariant mass distribution is then fit with the function F_{fit} of Eq. (3), once using F_{bkg}^a , and then using a different function F_{bkg}^b , given by Eq. (2). For each pseudo-experiment, the spurious signal yield, expressed by the number of events N_{bias}^a and N_{bias}^b , is determined. The quantity N_{bias}^a is on average consistent with zero within the statistical fluctuations. The quantity N_{bias}^b represents the number of spurious signal events that are found in the signal yield if the function F_{bkg}^b is used to describe the background, when the background itself is actually distributed according to F_{bkg}^a . The median of the distribution of the difference $N_{\text{bias}}^a - N_{\text{bias}}^b$ obtained from the pseudo-experiments is defined as the bias introduced by using the function F_{bkg}^b , relative to the tested mass m_A . This procedure is repeated for each function F_{bkg}^a among the functional forms listed above, and the largest bias is taken as the systematic uncertainty in the number of signal events obtained from the maximum likelihood fit, due to the choice of Eq. (2) to parametrize the background distribution. Choosing a different function F_{bkg}^b , instead of Eq. (2), was shown to lead to similar biases over the whole mass range.

An example of fits to the data with Eq. (3) is shown in Fig. 4 for two mass hypotheses, and assuming a narrow-width resonance ϕ decaying to two muons. The uncertainties in the integrated luminosity, in the signal efficiency, and in the background parametrization are taken into account as nuisance parameters.

7 Results

No evidence of Higgs bosons production beyond the SM production is observed in the mass range where the analysis has been performed (Fig. 4), and exclusion limits at 95% confidence level (CL) are determined. A maximum likelihood fit to the data, as explained in the previous section, is performed under the background only and the signal-plus-background hypotheses, where the background includes the expectation for the SM Higgs boson. The systematic uncertainties are incorporated as nuisance parameters in the likelihood.

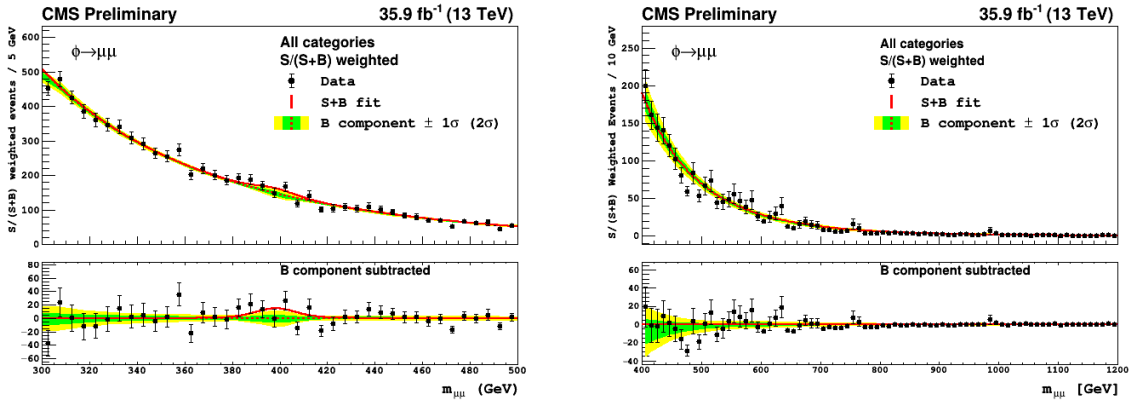


Figure 4: Examples of fits to data with a signal plus background hypothesis, for a narrow-width signal with the mass of 400 GeV (left), and 980 GeV (right), for the two event categories added together, after weighting by their sensitivity. The resonance ϕ is assumed to be produced via the b associated production, and to decay to two muons. The 68 and 95% CL bands, shown in green and light yellow, respectively, include the uncertainties in the background component of the fit. The lower panel shows the difference between the data and the background component of the fit.

The upper limits for the signal production are computed using the CL_s [70, 71] criterion and the hybrid frequentist-bayesian approach, where the distributions of the test-statistic are derived from pseudo-experiments[72].

The results are interpreted within the MSSM in the context of the $m_h^{\text{mod}+}$ and hMSSM scenarios, by combining both event categories. The 95% CL limit on the parameter $\tan \beta$ is presented as a function of m_A : the exclusion limit is chosen for each m_A as the $\tan \beta$ value at which the CL_s is lower than 0.05.

To estimate the impact of the various systematic uncertainties, the 95% CL limits have been determined by including different combination of uncertainties: statistical plus all systematic uncertainties, statistical plus systematic uncertainties on the fit bias, statistical plus systematic uncertainties on the efficiency. The comparison shows that the systematic uncertainties pertaining to the selection efficiency and the fit bias have similar impact.

The final results in terms of the expected 95% CL upper limit on the $m_h^{\text{mod}+}$ MSSM scenario, including the 68 and 95% CL bands, are shown in Fig. 5 (left), in the m_A – $\tan \beta$ plane. The results are obtained including the statistical and all systematic uncertainties. The 95% CL upper limit is computed up to $m_A = 600$ GeV, where the excluded $\tan \beta$ value exceeds 50. For higher values of $\tan \beta$ the MSSM predictions are no longer reliable. These results extend the excluded $\tan \beta$ range obtained at 7 and 8 TeV [18] and also extend the range of the tested m_A values from 300 to 600 GeV. The data are also interpreted in terms of the hMSSM model. The corresponding 95% CL upper limit on $\tan \beta$ as a function of m_A are shown in Fig. 5 (right). The observed limits are very similar in the two scenarios, since, in the m_A – $\tan \beta$ range covered by this analysis, the $m_h^{\text{mod}+}$ predictions for the h boson mass are consistent with the SM Higgs boson mass, and the cross sections of the H and A bosons are similar between the two models.

The results of the $\tau^+\tau^-$ analysis [25] exclude a much larger m_A – $\tan \beta$ region, reaching the value of $\tan \beta = 60$ at $m_A = 1.5$ TeV. For values of m_A up to 400 GeV the $\mu^+\mu^-$ results exclude a larger m_A – $\tan \beta$ region compared to the results of the $b\bar{b}$ analysis [28], which is instead slightly more sensitive at higher m_A reaching the value of $\tan \beta = 60$ at about $m_A = 700$ GeV.

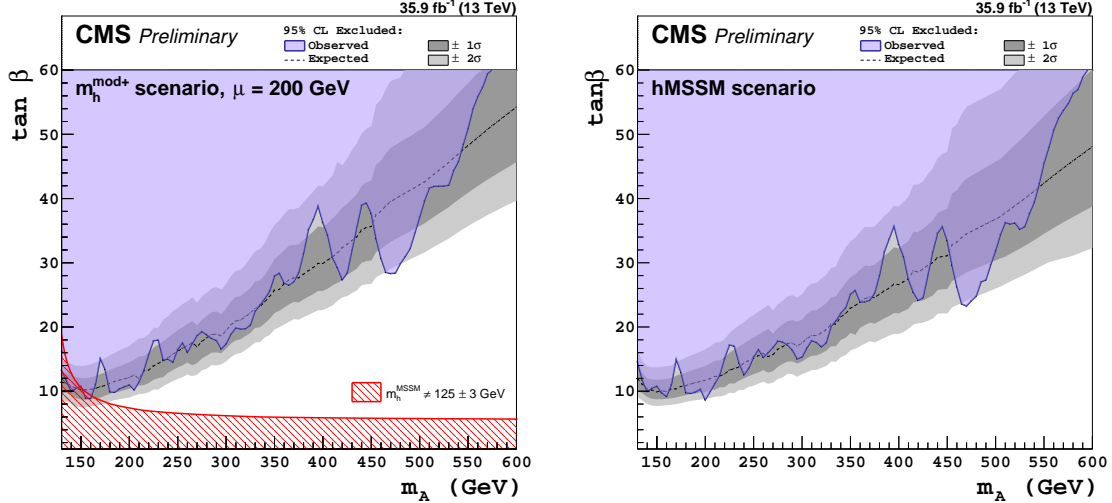


Figure 5: The 95% CL expected (including the 68 and 95% CL bands) and observed upper limits on $\tan \beta$ as a function of m_A for the $m_h^{\text{mod}+}$ (left) and the hMSSM (right) scenarios of the MSSM. The observed exclusion contour is indicated by the purple region, while the area under the red curve is excluded by requiring the neutral h boson mass consistent with 125 ± 3 GeV.

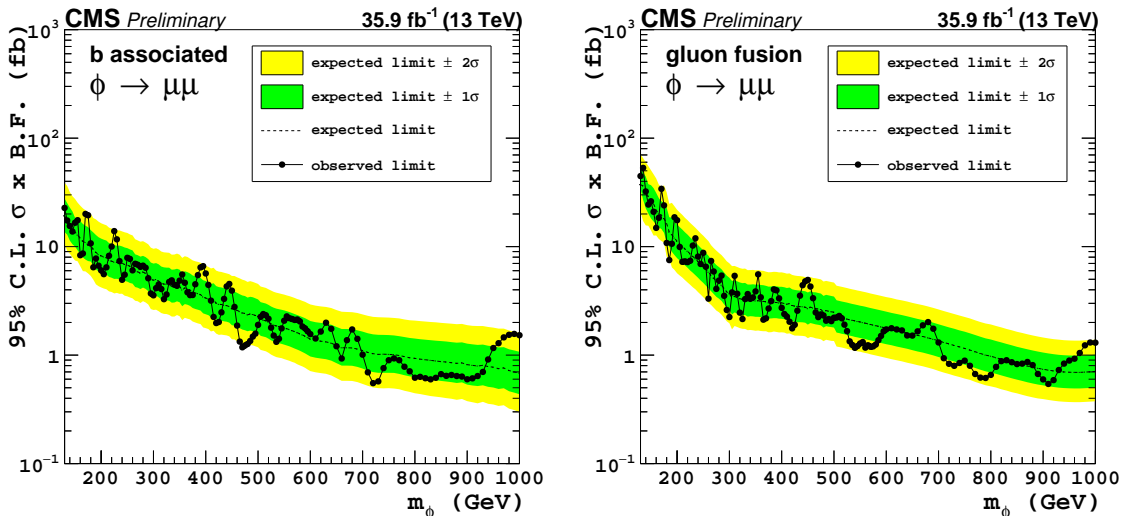


Figure 6: The 95% CL expected (including the 68 and 95% CL bands) and observed model-independent upper limits on the production cross section times branching fraction of a generic ϕ boson decaying to a dimuon pair, in the case of b associated (left) and gluon fusion (right) production. The results are obtained using a signal template with an intrinsic narrow-width.

Limits on the production cross section times decay branching fraction $\sigma \mathcal{B}(\phi \rightarrow \mu^+ \mu^-)$ for a single neutral scalar boson ϕ have been also determined. In the model-independent interpretation the ϕ boson is searched for as a single resonance with mass m_ϕ assuming a narrow-width or a width equal to 10% of m_ϕ . In the first case the intrinsic width of the signal is smaller than the invariant mass resolution, while in the second case the width is larger even for mass values near 1000 GeV (lower sensitivity of the analysis). The simulated signal of the A boson in the $\tan \beta = 5$ case (smallest intrinsic width, dominated by the detector resolution) is used as a template to compute the detection efficiency of a generic ϕ boson decaying to a muon pair. The ϕ boson is assumed to be produced entirely either via the b associated or the gluon fusion process, and the analysis is performed separately for the two production mechanisms. Figure 6 shows the 95% CL upper limits on the cross section times the decay branching fraction to $\mu^+ \mu^-$ as a function of the ϕ mass for a narrow resonance. These limits are more stringent by a factor 2-3 than those recently obtained by ATLAS in a similar search[19]. The corresponding upper limits assuming a signal template with a width equal to 10% of its mass value are shown in Fig. 7. In the case of large signal widths, the upper limits as a function of m_ϕ start from 140 GeV. This is done to have the signal peak $\pm 3\Gamma$ within the fit range. Moreover, as one may expect, the limits are less stringent than for the narrow-width approximation, and it is no longer possible to distinguish the fine structure of the 95% CL limits as a function of the mass, as observed for the narrow-width case.

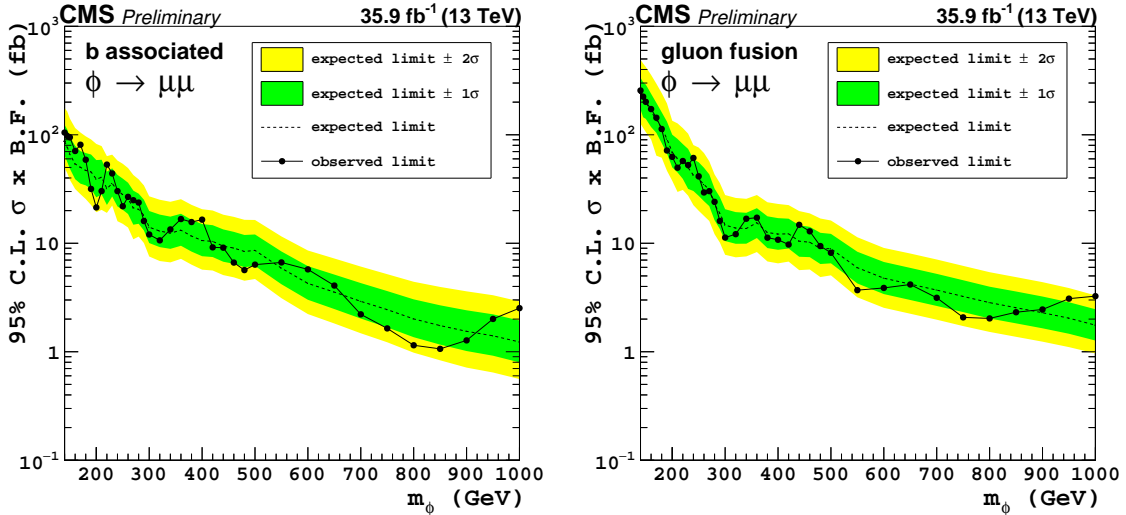


Figure 7: The 95% CL expected (including the 68 and 95% CL bands) and observed model-independent upper limits on the production cross section times branching fraction of a generic ϕ boson decaying to a dimuon pair, in the case of b associated (left) and gluon fusion (right) production. The results are obtained using a signal template with an intrinsic width equal to 10% of the nominal mass.

8 Summary

A search for neutral minimal supersymmetric standard model (MSSM) Higgs bosons decaying to $\mu^+ \mu^-$ was performed using 13 TeV data collected in proton-proton collisions by the CMS experiment at the LHC. No excess of events was found above the expected background due to Standard Model (SM) processes. The 95% CL upper limit for the production of beyond SM neutral Higgs bosons is determined in the framework of the $m_h^{\text{mod+}}$ and the hMSSM scenarios

of the MSSM. For the ratio of the vacuum expectation values of the neutral components of the two Higgs doublets, $\tan \beta$, the excluded values range from $\tan \beta \approx 10$ for the mass of the pseudoscalar A boson, $m_A = 130 \text{ GeV}$, to $\tan \beta \approx 60$ for $m_A \approx 600 \text{ GeV}$. The larger collected luminosity and the higher center-of-mass energy exclude a larger m_A – $\tan \beta$ region, compared to what was obtained at 7 and 8 TeV in a similar analysis. Model-independent exclusion limits on the production cross section times branching fraction of a generic narrow-width neutral boson decaying to two muons have been determined assuming the neutral boson to be produced entirely either via b associated or gluon fusion mechanisms. The limits are determined in the mass range from 130 to 1000 GeV, separately for the two production mechanisms. Similarly, exclusion limits are also obtained assuming a signal width equal to 10% of its mass value.

References

- [1] ATLAS Collaboration, “Observation of a new particle in the search for the Standard Model Higgs boson with the ATLAS detector at the LHC”, *Phys. Lett. B* **716** (2012) 1, doi:10.1016/j.physletb.2012.08.020, arXiv:1207.7214.
- [2] CMS Collaboration, “Observation of a new boson at a mass of 125 GeV with the CMS experiment at the LHC”, *Phys. Lett. B* **716** (2012) 30, doi:10.1016/j.physletb.2012.08.021, arXiv:1207.7235.
- [3] CMS Collaboration, “Observation of a new boson with mass near 125 GeV in pp collisions at $\sqrt{s} = 7$ and 8 TeV”, *JHEP* **06** (2013) 081, doi:10.1007/JHEP06(2013)081, arXiv:1303.4571.
- [4] ATLAS and CMS Collaborations, “Combined Measurement of the Higgs Boson Mass in pp Collisions at $\sqrt{s} = 7$ and 8 TeV with the ATLAS and CMS Experiments”, *Phys. Rev. Lett.* **114** (2015) 191803, doi:10.1103/PhysRevLett.114.191803, arXiv:1503.07589.
- [5] ATLAS and CMS Collaborations, “Measurements of the Higgs boson production and decay rates and constraints on its couplings from a combined ATLAS and CMS analysis of the LHC pp collision data at $\sqrt{s} = 7$ and 8 TeV”, *JHEP* **08** (2016) 045, doi:10.1007/JHEP08(2016)045, arXiv:1606.02266.
- [6] Yu. A. Golfand and E. P. Likhtman, “Extension of the algebra of Poincaré group generators and violation of p invariance”, *JETP Lett.* **13** (1971) 323.
- [7] J. Wess and B. Zumino, “Supergauge transformations in four-dimensions”, *Nucl. Phys. B* **70** (1974) 39, doi:10.1016/0550-3213(74)90355-1.
- [8] P. Fayet, “Supergauge invariant extension of the Higgs mechanism and a model for the electron and its neutrino”, *Nucl. Phys. B* **90** (1975) 104, doi:10.1016/0550-3213(75)90636-7.
- [9] P. Fayet, “Spontaneously broken supersymmetric theories of weak, electromagnetic and strong interactions”, *Phys. Lett. B* **69** (1977) 489, doi:10.1016/0370-2693(77)90852-8.
- [10] A. Djouadi, “The anatomy of electro-weak symmetry breaking. II. The Higgs bosons in the minimal supersymmetric model”, *Phys. Rept.* **459** (2008) 1, doi:10.1016/j.physrep.2007.10.005, arXiv:hep-ph/0503173.
- [11] M. Carena et al., “MSSM Higgs boson searches at the LHC: benchmark scenarios after the discovery of a Higgs-like particle”, *Eur. Phys. J. C* **73** (2013) 2552, doi:10.1140/epjc/s10052-013-2552-1, arXiv:1302.7033.
- [12] P. Bechtle et al., “Probing the Standard Model with Higgs signal rates from the Tevatron, the LHC and a future ILC”, *JHEP* **11** (2014) 039, doi:10.1007/JHEP11(2014)039, arXiv:1403.1582.
- [13] M. Carena et al., “Complementarity between nonstandard Higgs boson searches and precision Higgs boson measurements in the MSSM”, *Phys. Rev. D* **91** (2015) 035003, doi:10.1103/PhysRevD.91.035003, arXiv:1410.4969.

- [14] L. Maiani, A. D. Polosa, and V. Riquer, “Bounds to the Higgs sector masses in minimal supersymmetry from LHC data”, *Phys. Lett. B* **724** (2013) 274, doi:10.1016/j.physletb.2013.06.026, arXiv:1305.2172.
- [15] A. Djouadi et al., “The post-Higgs MSSM scenario: Habemus MSSM?”, *Eur. Phys. J. C* **73** (2013) 2650, doi:10.1140/epjc/s10052-013-2650-0, arXiv:1307.5205.
- [16] A. Djouadi et al., “Fully covering the MSSM Higgs sector at the LHC”, *JHEP* **06** (2015) 168, doi:10.1007/JHEP06(2015)168, arXiv:1502.05653.
- [17] ATLAS Collaboration, “Search for the neutral Higgs bosons of the minimal supersymmetric standard model in pp collisions at $\sqrt{s} = 7$ TeV with the ATLAS detector”, *JHEP* **02** (2013) 095, doi:10.1007/JHEP02(2013)095, arXiv:1211.6956.
- [18] CMS Collaboration, “Search for neutral MSSM Higgs bosons decaying to $\mu^+ \mu^-$ in pp collisions at $\sqrt{s} = 7$ and 8 TeV”, *Phys. Lett. B* **752** (2016) 221, doi:10.1016/j.physletb.2015.11.042, arXiv:1508.01437.
- [19] ATLAS Collaboration, “Search for scalar resonances decaying into $\mu^+ \mu^-$ in events with and without b -tagged jets produced in proton-proton collisions at $\sqrt{s} = 13$ TeV with the ATLAS detector”, arXiv:1901.08144.
- [20] ATLAS Collaboration, “Search for neutral Higgs bosons of the minimal supersymmetric standard model in pp collisions at $\sqrt{s} = 8$ TeV with the ATLAS detector”, *JHEP* **11** (2014) 056, doi:10.1007/JHEP11(2014)056, arXiv:1409.6064.
- [21] ATLAS Collaboration, “Search for minimal supersymmetric standard model Higgs bosons H/A and for a Z' boson in the $\tau\tau$ final state produced in pp collisions at $\sqrt{s} = 13$ TeV with the ATLAS detector”, *Eur. Phys. J. C* **76** (2016) 585, doi:10.1140/epjc/s10052-016-4400-6, arXiv:1608.00890.
- [22] ATLAS Collaboration, “Search for additional heavy neutral Higgs and gauge bosons in the ditau final state produced in 36 fb^{-1} of pp collisions at $\sqrt{s} = 13$ TeV with the ATLAS detector”, *JHEP* **01** (2018) 055, doi:10.1007/JHEP01(2018)055, arXiv:1709.07242.
- [23] CMS Collaboration, “Search for neutral minimal supersymmetric standard model Higgs bosons decaying to tau pairs in pp collisions at $\sqrt{s} = 7$ TeV”, *Phys. Rev. Lett.* **106** (2011) 231801, doi:10.1103/PhysRevLett.106.231801, arXiv:1104.1619.
- [24] CMS Collaboration, “Search for neutral Higgs bosons decaying to tau pairs in pp collisions at $\sqrt{s} = 7$ TeV”, *Phys. Lett. B* **713** (2012) 68, doi:10.1016/j.physletb.2012.05.028, arXiv:1202.4083.
- [25] CMS Collaboration, “Search for additional neutral MSSM Higgs bosons in the $\tau\tau$ final state in proton-proton collisions at $\sqrt{s} = 13$ TeV”, *JHEP* **08** (2018) 007, doi:10.1007/JHEP09(2018)007, arXiv:1803.06553.
- [26] CMS Collaboration, “Search for a Higgs boson decaying into a b-quark pair and produced in association with b quarks in proton-proton collisions at 7 TeV”, *Phys. Lett. B* **722** (2013) 207, doi:10.1016/j.physletb.2013.04.017, arXiv:1302.2892.

- [27] CMS Collaboration, “Search for neutral MSSM Higgs bosons decaying into a pair of bottom quarks”, *JHEP* **11** (2015) 071, doi:10.1007/JHEP11(2015)071, arXiv:1506.08329.
- [28] CMS Collaboration, “Search for beyond the standard model Higgs bosons decaying into a $b\bar{b}$ pair in pp collisions at $\sqrt{s} = 13$ TeV”, *JHEP* **08** (2018) 113, doi:10.1007/JHEP08(2018)113, arXiv:1805.12191.
- [29] ALEPH, DELPHI, L3, OPAL Collaborations, and the LEP Working Group for Higgs Boson Searches, “Search for neutral MSSM Higgs bosons at LEP”, *Eur. Phys. J. C* **47** (2006) 547, doi:10.1140/epjc/s2006-02569-7, arXiv:hep-ex/0602042.
- [30] CDF Collaboration, “Search for Higgs bosons predicted in two-higgs-doublet models via decays to tau lepton pairs in 1.96 TeV $p\bar{p}$ collisions”, *Phys. Rev. Lett.* **103** (2009) 201801, doi:10.1103/PhysRevLett.103.201801, arXiv:0906.1014.
- [31] CDF Collaboration, “Search for Higgs bosons produced in association with b -quarks”, *Phys. Rev. D* **85** (2012) 032005, doi:10.1103/PhysRevD.85.032005, arXiv:1106.4782.
- [32] D0 Collaboration, “Search for neutral Higgs bosons in the multi- b -jet topology in 5.2 fb^{-1} of $p\bar{p}$ collisions at $\sqrt{s} = 1.96$ TeV”, *Phys. Lett. B* **698** (2011) 97, doi:10.1016/j.physletb.2011.02.062, arXiv:1011.1931.
- [33] D0 Collaboration, “Search for Higgs bosons decaying to $\tau\tau$ pairs in $p\bar{p}$ collisions at $\sqrt{s} = 1.96$ TeV”, *Phys. Lett. B* **707** (2012) 323, doi:10.1016/j.physletb.2011.12.050, arXiv:1106.4555.
- [34] CMS Collaboration, “The CMS experiment at the CERN LHC”, *JINST* **3** (2008) S08004, doi:10.1088/1748-0221/3/08/S08004.
- [35] T. Sjöstrand et al., “An Introduction to PYTHIA 8.2”, *Comput. Phys. Commun.* **191** (2015) 159, doi:10.1016/j.cpc.2015.01.024, arXiv:1410.3012.
- [36] J. Alwall et al., “The automated computation of tree-level and next-to-leading order differential cross sections, and their matching to parton shower simulations”, *JHEP* **07** (2014) 079, doi:10.1007/JHEP07(2014)079, arXiv:1405.0301.
- [37] P. Nason, “A new method for combining NLO QCD with shower Monte Carlo algorithms”, *JHEP* **11** (2004) 040, doi:10.1088/1126-6708/2004/11/040, arXiv:hep-ph/0409146.
- [38] P. Artoisenet, R. Frederix, O. Mattelaer, and R. Rietkerk, “Automatic spin-entangled decays of heavy resonances in Monte Carlo simulations”, *JHEP* **03** (2013) 015, doi:10.1007/JHEP03(2013)015, arXiv:1212.3460.
- [39] NNPDF Collaboration, “Unbiased global determination of parton distributions and their uncertainties at NNLO and at LO”, *Nucl. Phys. B* **855** (2012) 153, doi:10.1016/j.nuclphysb.2011.09.024, arXiv:1107.2652.
- [40] CMS Collaboration, “Event generator tunes obtained from underlying event and multiparton scattering measurements”, *Eur. Phys. J. C* **76** (2016) 155, doi:10.1140/epjc/s10052-016-3988-x, arXiv:1512.00815.

- [41] GEANT4 Collaboration, “GEANT4-a simulation toolkit”, *Nucl. Instrum. Meth. A* **506** (2003) 250, doi:10.1016/S0168-9002(03)01368-8.
- [42] S. Heinemeyer, W. Hollik, and G. Weiglein, “FeynHiggs: A program for the calculation of the masses of the neutral CP-even Higgs bosons in the MSSM”, *Comput. Phys. Commun.* **124** (2000) 76, doi:10.1016/S0010-4655(99)00364-1, arXiv:hep-ph/9812320.
- [43] S. Heinemeyer, W. Hollik, and G. Weiglein, “The masses of the neutral CP-even Higgs bosons in the MSSM: Accurate analysis at the two-loop level”, *Eur. Phys. J. C* **9** (1999) 343, doi:10.1007/s100529900006, arXiv:hep-ph/9812472.
- [44] G. Degrassi et al., “Towards high-precision predictions for the MSSM Higgs sector”, *Eur. Phys. J. C* **28** (2003) 133, doi:10.1140/epjc/s2003-01152-2, arXiv:hep-ph/0212020.
- [45] M. Frank et al., “The Higgs boson masses and mixings of the complex MSSM in the Feynman-diagrammatic approach”, *JHEP* **02** (2007) 047, doi:10.1088/1126-6708/2007/02/047, arXiv:hep-ph/0611326.
- [46] T. Hahn et al., “High-precision predictions for the light CP-even Higgs boson mass of the minimal supersymmetric standard model”, *Phys. Rev. Lett.* **112** (2014) 141801, doi:10.1103/PhysRevLett.112.141801, arXiv:1312.4937.
- [47] LHC Higgs Cross Section Working Group Collaboration, “Handbook of LHC Higgs cross sections: 4. Deciphering the nature of the Higgs sector”, doi:10.23731/CYRM-2017-002, arXiv:1610.07922.
- [48] LHC Higgs Cross Section Working Group Collaboration, “Handbook of LHC Higgs cross sections: 3. Higgs properties”, doi:10.5170/CERN-2013-004, arXiv:1307.1347.
- [49] M. Czakon and A. Mitov, “Top++: A program for the calculation of the top-pair cross-section at hadron colliders”, *Comput. Phys. Commun.* **185** (2014) 2930, doi:10.1016/j.cpc.2014.06.021, arXiv:1112.5675.
- [50] R. Gavin, Y. Li, F. Petriello, and S. Quackenbush, “FEWZ 2.0: A code for hadronic Z production at next-to-next-to-leading order”, *Comput. Phys. Commun.* **182** (2011) 2388, doi:10.1016/j.cpc.2011.06.008, arXiv:1011.3540.
- [51] M. Aliev et al., “HATHOR: HAdronic Top and Heavy quarks crOss section calculatoR”, *Comput. Phys. Commun.* **182** (2011) 1034, doi:10.1016/j.cpc.2010.12.040, arXiv:1007.1327.
- [52] P. Kant et al., “HatHor for single top-quark production: Updated predictions and uncertainty estimates for single top-quark production in hadronic collisions”, *Comput. Phys. Commun.* **191** (2015) 74, doi:10.1016/j.cpc.2015.02.001, arXiv:1406.4403.
- [53] J. M. Campbell, R. K. Ellis, and C. Williams, “Vector boson pair production at the LHC”, *JHEP* **11** (2011) 018, doi:10.1007/JHEP07(2011)018, arXiv:1105.0020.
- [54] CMS Collaboration, “Particle-flow reconstruction and global event description with the CMS detector”, *JINST* **12** (2017) P10003, doi:10.1088/1748-0221/12/10/P10003, arXiv:1706.04965.

[55] CMS Collaboration, “Performance of CMS muon reconstruction in pp collision events at $\sqrt{s} = 7$ TeV”, *JINST* **7** (2012) P10002, doi:10.1088/1748-0221/7/10/P10002, arXiv:1206.4071.

[56] CMS Collaboration, “Performance of the CMS muon detector and muon reconstruction with proton-proton collisions at $\sqrt{s} = 13$ TeV”, *JINST* **13** (2018) P06015, doi:10.1088/1748-0221/13/06/P06015, arXiv:1804.04528.

[57] M. Cacciari, G. P. Salam, and G. Soyez, “The anti- k_t jet clustering algorithm”, *JHEP* **04** (2008) 063, doi:10.1088/1126-6708/2008/04/063, arXiv:0802.1189.

[58] M. Cacciari, G. P. Salam, and G. Soyez, “FastJet user manual”, *Eur. Phys. J. C* **72** (2012) 1896, doi:10.1140/epjc/s10052-012-1896-2, arXiv:1111.6097.

[59] K. Rose, “Deterministic annealing for clustering, compression, classification, regression, and related optimization problems”, *Proceedings of the IEEE* **86** (1998) 2210, doi:10.1109/5.726788.

[60] M. Cacciari, G. P. Salam, and G. Soyez, “The anti- k_t jet clustering algorithm”, *JHEP* **04** (2008) 063, doi:10.1088/1126-6708/2008/04/063, arXiv:0802.1189.

[61] CMS Collaboration, “Identification of heavy-flavour jets with the CMS detector in pp collisions at 13 TeV”, *JINST* **13** (2018) P05011, doi:10.1088/1748-0221/13/05/P05011, arXiv:1712.07158.

[62] CMS Collaboration, “The CMS trigger system”, *JINST* **12** (2017) P01020, doi:10.1088/1748-0221/12/01/P01020, arXiv:1609.02366.

[63] M. Cacciari and G. P. Salam, “Pileup subtraction using jet areas”, *Phys. Lett. B* **659** (2008) 119, doi:10.1016/j.physletb.2007.09.077, arXiv:0707.1378.

[64] CMS Collaboration, “W-like measurement of the z boson mass using dimuon events collected in pp collisions at $\sqrt{s} = 7$ TeV”, CMS Physics Analysis Summary CMS-PAS-SMP-14-007, 2017.

[65] CMS Collaboration, “Measurement of the inelastic proton-proton cross section at $\sqrt{s} = 13$ TeV”, *JHEP* **07** (2018) 161, doi:10.1007/JHEP07(2018)161, arXiv:1802.02613.

[66] ATLAS Collaboration, “Measurement of the inelastic proton-proton cross section at $\sqrt{s} = 13$ TeV with the ATLAS detector at the LHC”, *Phys. Rev. Lett.* **117** (2016) 182002, doi:10.1103/PhysRevLett.117.182002, arXiv:1606.02625.

[67] CMS Collaboration, “Determination of jet energy calibration and transverse momentum resolution in CMS”, *JINST* **6** (2011) P11002, doi:10.1088/1748-0221/6/11/P11002, arXiv:1107.4277.

[68] CMS Collaboration, “CMS luminosity measurements for the 2016 data taking period”, CMS Physics Analysis Summary CMS-PAS-LUM-17-001, 2017.

[69] CMS Collaboration, “Search for the Higgs boson decaying to two muons in proton-proton collisions at $\sqrt{s} = 13$ TeV”, *Phys. Rev. Lett.* **122** (2019) 021801, doi:10.1103/PhysRevLett.122.021801, arXiv:1807.06325.

[70] T. Junk, “Confidence level computation for combining searches with small statistics”, *Nucl. Instrum. Meth. A* **434** (1999) 435, doi:10.1016/S0168-9002(99)00498-2, arXiv:hep-ex/9902006.

- [71] A. L. Read, “Presentation of search results: The CL_s technique”, *J. Phys. G* **28** (2002) 2693, doi:10.1088/0954-3899/28/10/313.
- [72] ATLAS, CMS, LHC Higgs Combination Group Collaboration, “Procedure for the LHC Higgs boson search combination in summer 2011”.